TOPICAL REVIEW — Magnetism, magnetic materials, and interdisciplinary research

Mn-based antiperovskite functional materials: Review of research*

Tong Peng(童 鹏)[a], Wang Bo-Sen(王铂森)[a], and Sun Yu-Ping(孙玉平)[a,b]†

[a] Key Laboratory of Materials Physics, Institute of Solid State Physics, Chinese Academy of Sciences, Hefei 230031, China
[b] High Magnetic Field Laboratory, Chinese Academy of Sciences, Hefei 230031, China

(Received 26 April 2013)

Our recent research on the Mn-based antiperovskite functional materials $AX\mathrm{Mn_3}$ (A: metal or semiconducting elements; X: C or N) is outlined. Antiperovskite carbides (e.g., $\mathrm{AlCMn_3}$) show large magnetocaloric effect comparable to those of typical magnetic refrigerant materials. Enhanced giant magnetoresistance up to 70% at 50 kOe (1 Oe = 79.5775 A·m^{-1}) over a wide temperature span was obtained in $\mathrm{Ga_{1-x}Zn_xCMn_3}$ and $\mathrm{GaCMn_{3-x}Ni_x}$. In $\mathrm{Cu_{0.3}Sn_{0.5}NMn_{3.2}}$, negative thermal expansion (NTE) was achieved in a wide temperature region covering room temperature ($\alpha = -6.8$ ppm/K, 150 K–400 K). Neutron pair distribution function analysis suggests the Cu/Sn-Mn bond fluctuation is the driving force for the NTE in $\mathrm{Cu_{1-x}Sn_xNMn_3}$. In $\mathrm{CuN_{1-x}C_xMn_3}$ and $\mathrm{CuNMn_{3-y}Co_y}$, the temperature coefficient of resistivity (TCR) decreases monotonically from positive to negative as Co or C content increases. TCR is extremely low when the composition approaches the critical points. For example, TCR is $\sim$ 1.29 ppm/K between 240 K and 320 K in $\mathrm{CuN_{0.95}C_{0.05}Mn_3}$, which is one twentieth of that in the typical low-TCR materials ($\sim$ 25 ppm/K). By studying the critical scaling behavior and X deficiency effect, some clues of localized-electron magnetism have been found against the background of electronic itinerant magnetism.

Keywords: antiperovskite, magnetocaloric effect, giant magnetoresistance, negative thermal expansion

PACS: 75.20.En, 75.30.Sg, 75.47.De **DOI:** 10.1088/1674-1056/22/6/067501

1. Introduction

Over the past several decades, perovskite oxides RMO_3 (R = rare earth or alkaline element, M = transition metal) have been studied extensively due to their many and diverse novel phenomena such as high transition temperature superconductivity,[1] ferroelectrics,[2] and colossal magnetoresistance (CMR).[3] In contrast, relatively less attention has been paid to the antiperovskite materials. Among the antiperovskite family, the Mn-based ones (Fig. 1) with general formula $AX\mathrm{Mn_3}$ (A: metal or semiconducting elements, X: C or N) is a large group of magnetic materials with a great variety of magnetic structures and magnetic transitions.[4] Beginning in the 1960s, the basic properties of $AX\mathrm{Mn_3}$ have been extensively studied via neutron diffraction,[5,6] NMR,[7,8] specific heat measurements,[9] and bulk magnetic susceptibility measurements.[10–12] Just recently, particularly after the discovery of superconductivity in the isostructural Ni-based antiperovskite $\mathrm{MgCNi_3}$,[13] the Mn-based antiperovskites started to get renewed attention and new functionalities were continuously reported, such as giant magnetoresistance (GMR),[14,15] large magnetocaloric effect (MCE),[16–18] negative or zero thermal expansion (NTE or ZTE),[19–24] nearly zero temperature coefficient of resistance (TCR),[25–27] and giant magnetostriction (MS).[28] Unlike their perovskite counterparts (i.e., $R\mathrm{MnO_3}$), the $AX\mathrm{Mn_3}$ compounds behave like metals, having metallic conductivity, good thermal conductivity, and good mechanical properties.[19,29] Besides, the antiperovskite $AX\mathrm{Mn_3}$ compounds are made of cheap and non-toxic constituents. These advantages are favorable to the potential applications of $AX\mathrm{Mn_3}$ in relevant fields where metallic features (e.g., high electrical or thermal conductivity, high stiffness, etc.) would be desirable.

In $AX\mathrm{Mn_3}$, the Mn 3d orbitals contribute mainly to the electronic density of states (DOS) at the Fermi energy (E_F), while the X p–Mn d hybridization leads to a wide conduction band crossing over the E_F.[30] From the view of real space, the magnetic couplings via Mn–X–Mn channels may compete with the direct Mn–Mn interactions.[31,32] The Mn 3d electrons simultaneously participate in both conductive and magnetic phenomena. Similar to manganites, the antiperovskite $AX\mathrm{Mn_3}$ exhibits universally strong coupling among lattice, spin, and charge carriers, especially in the vicinity of magnetic transitions.[33] Moreover, the three-dimensional network constructed by corner-sharing $\mathrm{Mn_6}X$ octahedra contains three-dimensional geometrical frustration in terms of magnetic interactions.[34] The strong couplings among the various degrees of freedoms and the competing magnetic interactions that are close in energy make the physical properties of $AX\mathrm{Mn_3}$ compounds sensitive to subtle changes in chemical composition,[35] temperature, pressure,[36,37] and external magnetic field.[10,37] Such a complex physical background provides good opportunity to adjust the functionalities to meet

*Project supported by the National Natural Science Foundation of China (Grant Nos. 11174295, 51001094, 91222109, 51171177, and 50701042) and the National Key Basic Research of China (Grant No. 2011CBA00111).

†Corresponding author. E-mail: ypsun@issp.ac.cn

© 2013 Chinese Physical Society and IOP Publishing Ltd

the requirements of practical applications, even though it is currently a challenge to comprehend the abundant physical properties mentioned above in a unified way.

In this review, we introduce our recent progress in exploring and improving the functionalities in $AXMn_3$ materials by manipulating the chemical compositions, as well as in studying the mechanisms underlying the related physical properties and functionalities.

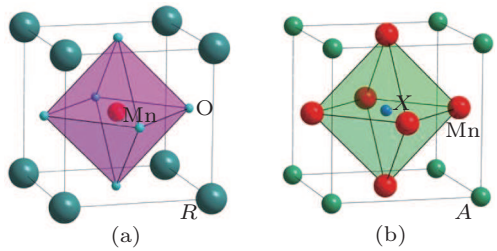


Fig. 1. (a) Perovskite manganites $RMnO_3$ (R: rare earth or alkaline element). (b) Antiperovskite $AXMn_3$ (A: metal or semiconducting elements, X: C or N). Note that the Mn atom is located at the center of the MnO_6 octahedron in $RMnO_3$, but at the corners of the MnX_6 octahedron in $AXMn_3$. Thus the latter structure is called "antiperovskite."

2. Giant magnetoresistance (GMR) in Mn-based antiperovskite carbides

$GaCMn_3$ is a prototype antiperovskite compound that has received extensive studies. Now it is known that it undergoes three magnetic transitions upon cooling: a paramagnetic (PM)–ferromagnetic (FM) transition at $T_C \sim 246$ K, an FM-intermediate magnetic phase (IM) transition at $T_{F-I} \sim 160$ K, and finally an IM-antiferromagnetic (AFM) transition with a discontinuous lattice expansion in volume at $T_{I-A} \sim 158$ K. The IM state consists of both AFM and FM components, probably forming a canted spin configuration.[14] However, the FM and IM phases are undistinguishable by bulk magnetization measurements in $GaCMn_3$. A plateau-like temperature dependence of GMR has been observed with the maximum MR value of 50% at 50 kOe (1 Oe = 57.5775 A·m^{-1}), covering a temperature range of about 20 K.[33] Phenomenologically, the GMR is associated with the field-induced AFM–FM (or IM) transition (noted as AFM–FM/IM hereafter) where a strong correlation among lattice, spin, and charge exists. GMR with larger temperature spans could be observed if the AFM ground state can be effectively suppressed by external magnetic field. However, it was shown by K. Kamishima *et al.* that a magnetic field as high as 240 kOe is required to suppress the AFM ground state.[14] Chemical substitution (chemical alloying) provides a possible way to improve the GMR in $GaCMn_3$ for instance, to enhance the GMR value, to expand the temperature span, and to reduce the operational magnetic field. To this end, we studied the MR effect in doped $GaCMn_3$, i.e., in $GaCMn_{3-x}Ni_x$ ($0 \le x \le 0.1$)[38] and $Ga_{1-x}Zn_xCMn_3$ ($0 \le x \le 0.3$).[39]

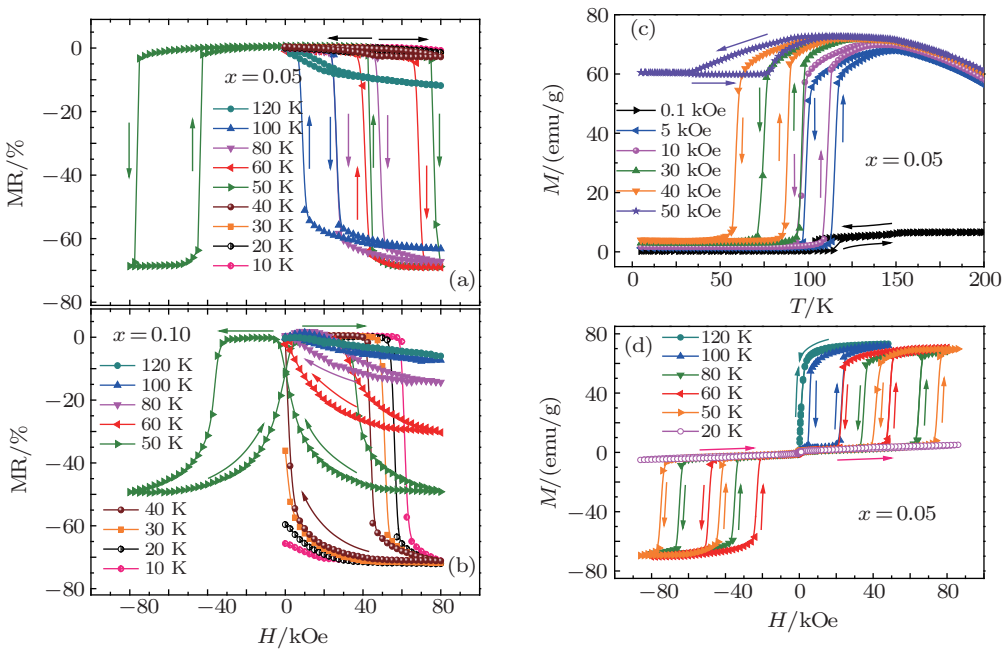


Fig. 2. Magnetoresistance MR(H) for $GaCMn_{3-x}Ni_x$ with $x = 0.05$ (a) and 0.1 (b). Magnetization $M(T)$ measured at different fields with both warming and cooling processes for $x = 0.05$ (c). Field-dependent magnetization $M(H)$ measured at selected temperatures for $x = 0.05$ (d).[38]

Figures 2(a) and 2(b) display the field dependence of magnetoresistivity (MR) [defined as $MR = (\rho_H - \rho_0)/\rho_0$] at selected temperatures with the magnetic field up to 85 kOe for $GaCMn_{3-x}Ni_x$ with $x = 0.05$ and 0.1, respectively.[38] For $x = 0.05$, in a wide range from 50 K to 100 K, the MR exceeds 60%, and the largest MR value at 50 K and 60 K exceeds

70%. Further, at 100 K, a completely recoverable saturated MR of 65% can be achieved in a magnetic field of 40 kOe. The MR values and temperature spans are increased significantly compared with the parent $GaCMn_3$. As to $x = 0.1$, MR can reach 70% below 40 K with a larger hysteresis than observed in $x = 0.05$. The hysteresis indicates the field-induced transition is of the first order. As shown in Fig. 2(c), an abrupt change in $M(T)$ around T_{I-A} is clearly seen and the $M(T)$ is remarkably enhanced at low temperatures when the magnetic field is higher than 50 kOe. As shown in Fig. 2(d), between 50 K and 120 K (below T_{I-A} in zero field), the $M(H)$ shows a sharp transition at a certain magnetic field, from the low-magnetization AFM to the high-magnetization IM/FM phase with a magnetization change of ~ 70 emu/g. Above 120 K, the curves exhibit FM behavior, corresponding to the small MR values ($< 20\%$) as shown in Fig. 2(a). The $M(H)$ at 20 K, where no MR was obtained, exhibits AFM behavior without abrupt magnetization changes up to 85 kOe. This clearly indicates that the GMR observed is closely related to the field-induced AFM–IM/FM transition. In the parent $GaCMn_3$, the measurement of the Hall effect reveals that the average carrier density (electron-type) in the FM/IM phase is about five times larger than that in the AFM phase.[14] The substitution of Ni for Mn in $GaCMn_3$ can be seen as electron-type doping, which favors the FM/IM state at the expense of the AFM ground state. Consequently, the slight Ni-doping weakens the rigid AFM ground state and favors the field-induced AFM–FM transition, leading to the enhanced GMR.

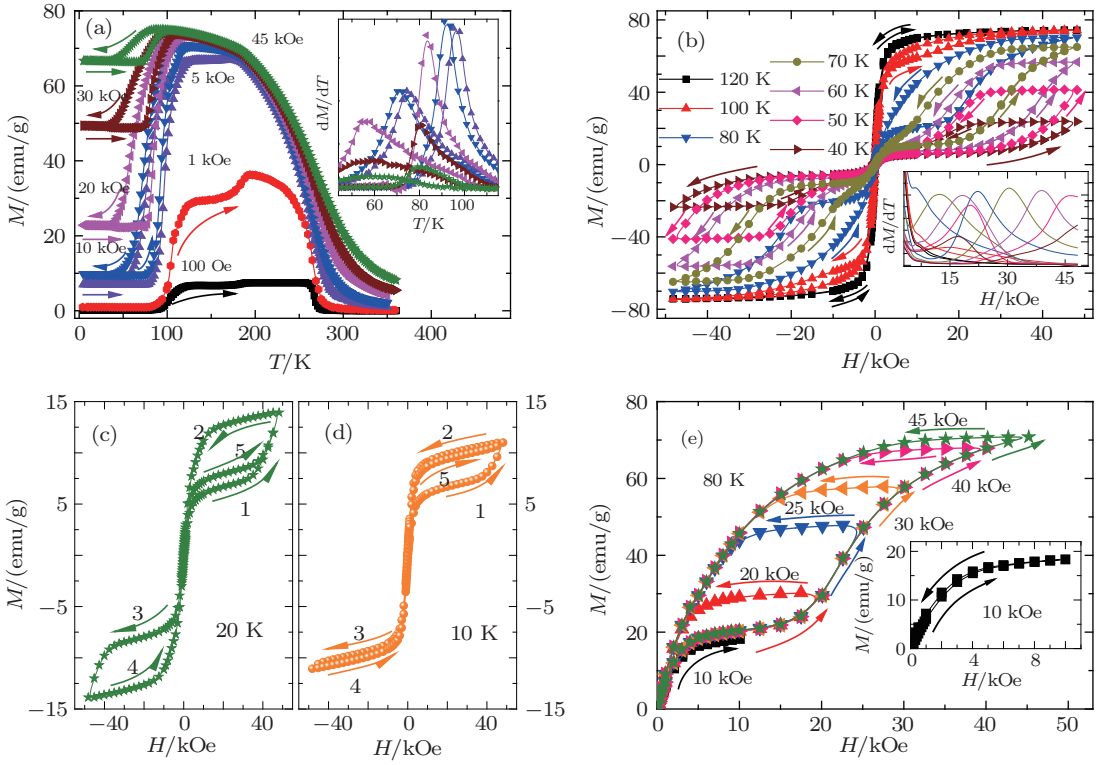


Fig. 3. (a) $M(T)$ for $Ga_{0.8}Zn_{0.2}CMn_3$ under both field-cooled cooling and field-cooled warming processes at different magnetic fields. Inset shows the plots of dM/dT versus T. (b) $M(H)$ at several selected temperatures from 120 K to 40 K. Inset shows the plots of dM/dH versus H. (c) $M(H)$ curve at 20 K. (d) $M(H)$ curve at 10 K. (e) MHLs initiated during both the ascending-field cycle and the descending-field cycle at different fields. Inset shows the $M(H)$ curve at 10 kOe. The arrows indicate the direction of temperature or magnetic field variation.[39]

The MR effect was also investigated for $Ga_{1-x}Zn_xCMn_3$ with $0 \leq x \leq 0.3$. In the intermediate doping level around $x = 0.2$, the MR effect is optimized with highest MR value of 60% at 40 kOe covering a broad temperature region.[39] The $x = 0.2$ composition was thus subjected to further measurements. Although the MR effect is similar to that observed in $GaCMn_{3-x}Ni_x$, our detailed magnetization analysis indicates a more complex nature of the field-induced magnetic transition in $Ga_{0.8}Zn_{0.2}CMn_3$. As shown in Fig. 3(a), the IM and FM states are well distinguished under low measurement fields. In the $M(T)$ curve measured at 1 kOe, three magnetic transitions were found at $T_C \sim 265$ K, $T_{F-I} \sim 190$ K, and the AFM–IM at $T_{I-A} \sim 100$ K. Both T_{F-I} and T_{I-A} shift to lower temperatures with increased magnetic field, while the T_C increases. Meanwhile, the $M(T)$ below T_{I-A} increases gradually as the magnetic field increases, in contrast to the sharp transition observed in Ni-doped samples. Similarly, the gradual magnetization change can be found in $M(H)$ curves measured below

100 K [Fig. 3(b)]. This indicates that the magnetic transformation induced by external field is rather incomplete under moderate magnetic fields. Furthermore, the magnetization was not saturated even at 48 kOe below 100 K, and a large hysteresis can be seen. More interestingly, for 20 K and 10 K, the virgin curve lies outside the envelope curve, as shown in Figs. 3(c) and 3(d). After the first field cycling, the original state is lost and cannot be restored again. A similar behavior has been observed around a first-order AFM–FM transition in many intermetallic compounds, where the supercooling and kinetic arrest effects are responsible for this characteristic.[40] In addition, in order to address the complicated ground state and the AFM–IM transition, the minor hysteresis loops (MHLs) at 80 K were measured, a method that has been widely adopted to investigate phase coexistence.[40] As shown in Fig. 3(e), for the maximum H_{max} of 10 kOe, the minor loop of the original curve is completely reversible. As the H_{max} exceeds 15 kOe, magnetic hysteresis occurs and the loop becomes larger and larger with increasing H_{max}. The hysteresis is not due to domain wall pinning or rotation because it is not visible at zero field. The intrinsic MHLs imply the incomplete transition between the competing magnetic phases in the vicinity of a first-order magnetic transition induced by magnetic field. In other words, the field-induced AFM–FI transition is characterized by phase coexistence and metastability.

A comparison study of the low-temperature specific heat was performed for $GaCMn_3$ and $Ga_{0.8}Zn_{0.2}CMn_3$ at different magnetic fields.[39] It was found that the substitution of Zn for Ga leads to a significant increase of the electronic specific coefficient γ from 21.13 mJ/mol·K^2 for $GaCMn_3$ to 32.16 mJ/mol·K for $Ga_{0.8}Zn_{0.2}CMn_3$. As confirmed in $GaCMn_3$, the carrier density of the FM (FI) state is five times larger than in the AFM ground state.[14] Therefore, the observed change of γ is a signature of change of the ground state: namely, the FM interactions must be enhanced in the ground state at the expense of the AFM interaction. For $Ga_{0.8}Zn_{0.2}CMn_3$, the γ increases from 32.16 mJ/mol·K^2 at zero field to 39.06 mJ/mol·K^2 at 85 kOe, indicating a further suppression of the AFM ground state. These results can be understood as follows: the super-zone gap may be formed in the AFM state with a small value of DOS near the Fermi level.[41] At 85 kOe, the AFM state was replaced by the IM state, resulting in an increase of the DOS at E_F. However, for $GaCMn_3$, the change of γ is quite small at 50 kOe, indicating a rigid AFM ground state, which refers to the relatively small MR. In conclusion, it is thought that the metastability of the AFM–IM transition and enhanced GMR in $Ga_{1-x}Zn_xCMn_3$ are highly relevant to reconstruction of the electronic band structure in magnetic fields.

The GMR values in the Zn and Ni-doped samples rank among the largest ever observed in 3d GMR systems, such as FM shape memory alloys $Ni_{50}Mn_{50-x}In_x$ ($x = 14$–16) (MR$\sim$ 70% at 50 kOe)[42] and $Mn_2Sb_{1-x}Sn_x$ ($0 < x \leq 0.4$) (60% at 50 kOe).[43] Our result proves that the chemical substitution can be employed to effectively optimize the MR effect in $GaCMn_3$. However, the underlying mechanisms are still not well understood. According to the results of neutron diffraction for $GaCMn_3$,[5] the Mn moments in each (111) plane are parallel along the [111] direction, while the spins on the adjacent (111) planes are anti-parallel in the AFM phase and parallel in the FM phase. But the magnetic structure in the IM phase is rather complex. Clearly, the spin configuration (arrangement) is also closely associated with the AFM–IM/FM transition. A detailed mapping of the magnetic/structural evolutions with composition, temperature, and magnetic field would help explain the enhanced GMR in the doped $GaCMn_3$ samples.

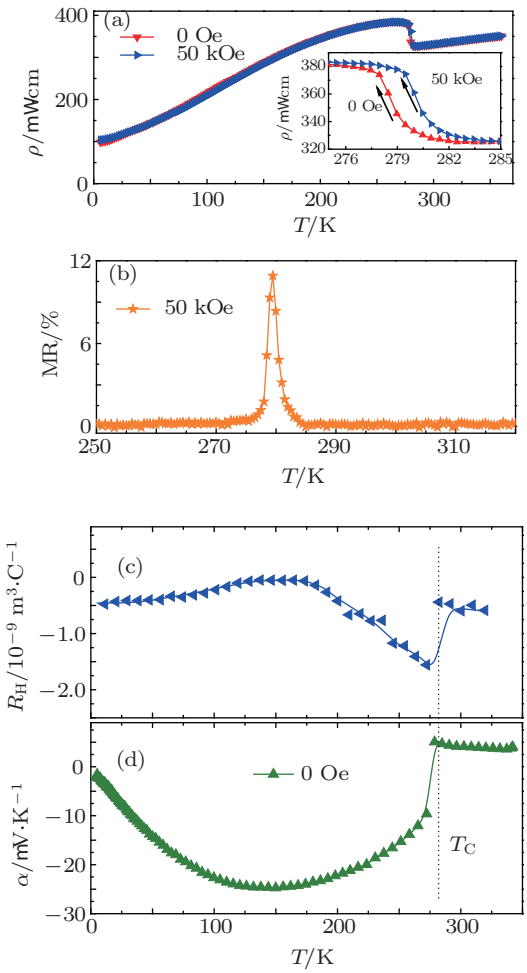


Fig. 4. Resistivity measured at both zero and 50 kOe (a), magnetoresistance (b), normal Hall coefficient (c), and Seebeck coefficient (d) for $SnCMn_3$.[44] Inset of panel (a) shows the area near the ferrimagnetic transition (T_C). The vertical dotted line in panels (c) and (d) shows the position of T_C.

Unlike $GaCMn_3$, $SnCMn_3$ undergoes only one magnetic transition from PM to ferrimagnetic (FI) state at $T_C \sim 279$ K with an isostructural transformation of the cubic lattice.[4] An early report showed a positive MR effect (less than

4% at 50 kOe) and indicated the magnetic scattering processes may not be the principal interaction mechanism in this compound.[15] In addition, the substitution of Zn for Sn in $SnCMn_3$ reduced T_C, accompanying a large negative MR of 34% at 120 kOe.[15] Recently, we revisited the structural, magnetic, and electrical transport properties of $SnCMn_3$. Compared with the earlier reports, the sharp magnetic transition ($\Delta T \sim 3$ K), low residual resistivity (96 μΩ·cm) and the relatively high residual resistivity ratio [RRR = ρ(300 K)/ρ(5 K) = 3.4] indicate that the quality of our sample is relatively good (see Fig. 4(a)).[44] Accordingly, a relatively large positive MR of $\sim$ 11% at 50 kOe around T_C was observed as shown in Fig. 4(b).

In addition, both the normal Hall coefficient $R_H(T)$ (Fig. 4(c)) and the Seebeck coefficient $S(T)$ (Fig. 4(d)) show abrupt changes at T_C, indicating a sudden reconstruction of the electronic structure, e.g., the DOS near E_F. Together with the lattice volume collapse at T_C,[36] our results suggest a close correlation among the different degrees of freedom, such as spin, lattice, and charge carrier. The charge carrier density estimated by $R_H(T)$ in the high-temperature PM phase is triple that in the low-temperature FI phase.[45] Under external magnetic field, the FI–PM transition is shifted to lower temperatures. As a result, the large MR occurs due to the difference in the charge carrier density between the FI and PM phases. In addition, the interaction among spin, lattice, and charge seems to be universal in $AXMn_3$ compounds since sudden magnetic/structural phase transitions have been widely observed.

In the doped samples $SnCMn_{3-x}Fe_x$, positive MR was observed around the FI–PM transition.[46] Both the Curie temperature T_C and saturated magnetization are reduced with increasing Fe concentration x. This can be attributed to the reduction of the electronic density of states at E_F by Fe-doping. As a result of the broadening of the FI–PM transition upon Fe doping, the peak value of the MR decreases to 3.2% for $x = 0.2$.

3. Large magnetocaloric effect (MCE) in Mn-based antiperovskite carbides

Magnetic refrigeration based on the MCE has attracted great attention because it is more environment-friendly and energy-efficient than the traditional vapor-cycle refrigeration technology.[47] Up to now, several typical refrigerant materials have been developed that show excellent MCE, such as Gd–Si–Ge,[48] Mn–As,[49] La–Fe–Si,[50] manganites oxides,[51] and Heusler alloys.[52] The exploration of new MCE material systems with low-cost and eco-friendly materials and high refrigerant capability would enrich the study of the MCE itself and offer candidate refrigerants for practical application in magnetic refrigeration.

In 2003, the giant negative MCE was discovered in antiperovskite $GaCMn_3$.[16] The MCE is related with the first-order AFM–IM transition at $\sim$ 159 K. Interestingly, both the value of the isothermal magnetic entropy changes ($-\Delta S_M$) and the adiabatic temperature change (ΔT_{ad}) show plateau-like temperature dependencies with maximum values of about 15 J/kg·K and 5.4 K at $\Delta H = 20$ kOe, respectively. The $-\Delta S_M$ value is almost unchangeable but the temperature span broadens significantly with increasing magnetic field. However, the thermal hysteresis due to the first-order transition adversely affects the reversibility of the MCE and the usefulness of the material as a magnetic refrigerant. In comparison with the first-order AFM–IM transition, little attention has been paid to the MCE with respect to the second-order FM–PM transition at $T_C \sim 246$ K which is close to room temperature. Therefore, in order to explore new room-temperature MEC materials, we investigated the MCE around T_C in $Ga_{1-x}CMn_{3+x}$,[53] $Ga_{1-x}Al_xCMn_3$,[54] $GaCMn_{3-x}Ni_x$[55] and in related materials $AlCMn_3$[56] and $Sn_{1-x}CMn_{3+x}$[45,57] with T_C close to room temperature. The entropy change ΔS_M induced by the variation of a magnetic field from 0 to H was calculated based on classical thermo-dynamical theory and Maxwell's relation.[16,45]

In $Ga_{1-x}CMn_{3+x}$,[53] the T_C is increased from 250 K for $x = 0$ to 323 K for $x = 0.08$. Although the maximum magnetic entropy change $-\Delta S_M^{max}$ reduces with increasing x, the $-\Delta S_M(T)$ peak becomes wide and exhibits a table-like temperature dependence for $x = 0.08$ (Fig. 5). The temperature span is about 160 K and includes room temperature. The value of $-\Delta S_M^{max}$ is about 4.19, 2.65, 2.39, and 1.81 J/kg·K for $x = 0$, 0.06, 0.07, and 0.08 with $\Delta H = 45$ kOe, respectively. Such a table-like shape behavior of $-\Delta S_M(T)$ is beneficial to the actual magnetic refrigerant applications. The relative cooling power (RCP) is a measure of how much heat can be transferred between the cold and hot sinks in an ideal refrigerant cycle, and thus a critical criterion for selecting potential substances to serve as magnetic refrigerants. RCP can be calculated by taking the formula[53] $RCP = -\Delta S_M^{max} \delta T_{FWHM}$, where δT_{FWHM} is the full width at half maximum (FWHM) of the $\Delta S_M(T)$ peak. The values of RCP at 45 kOe increase with increasing x from 0 to 0.07 and gradually decrease with further increasing x. This behavior is attributed to the competing contributions from $-\Delta S_M^{max}$ and δT_{FWHM}. The largest RCP is about 301 J/kg around 296.5 K with $\Delta H = 45$ kOe. It is nearly 40% larger than that of parent $GaCMn_3$ ($\sim$ 218 J/kg, at 250 K) with the same magnetic field change. As to $Ga_{1-x}Al_xCMn_3$, the values of $-\Delta S_M^{max}$ with ΔH= 45 kOe decreases from 4.19 J/kg·K for $x = 0$ to 2.11 J/kg·K for $x = 0.15$.[54] Similar to $Ga_{1-x}CMn_{3+x}$, the RCP increases gradually due to the broadening of $-\Delta S_M(T)$ peak as Al concentration increases. Specially, for $x = 0.15$, the RCP reaches the maximum value

293 J/kg at $\sim$ 312 K. In addition, Ni substitution for Mn can also enhances the RCP in $GaCMn_3$ significantly by increasing the $-\Delta S_M(T)$ peak width. In $GaCMn_{2.9}Ni_{0.1}$, the RCP is 285.5 J/kg with $\Delta H = 45$ kOe at around 260 K.[55]

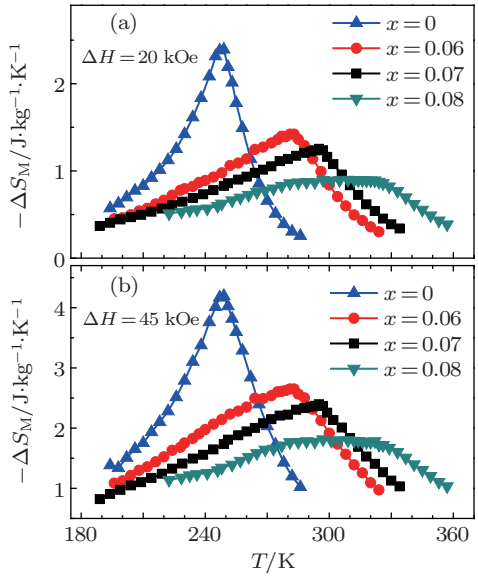


Fig. 5. Magnetic entropy change $-\Delta S_M(T)$ as a function of temperature under magnetic field changes of $\Delta H = 20$ kOe (a) and 45 kOe (b) for $Ga_{1-x}CMn_{3+x}$.[53]

$AlCMn_3$ is an FM material with $T_C \sim 288$ K.[7] In order to study the MCE, we prepared a polycrystalline sample of $AlCMn_3$ by standard solid state reaction.[56] The lattice parameter (0.3873 nm) and T_C (289 K) are consistent with those reported by other authors.[7] The magnetic transition at T_C was confirmed to be second-order transition without thermal hysteresis. As shown in Fig. 6(a), the maximum magnetic entropy change $-\Delta S_M^{max}$ reaches 3.28 J/kg·K for $\Delta H = 45$ kOe. Furthermore, the value of ΔT_{ad} was also calculated from the measurement of the specific heat by using the formula $\Delta T_{ad} = -\Delta S_M(T,H)T/C_P(T,H)$, where $C_P(T,H)$ is zero-field specific heat. With increasing ΔH, the values of $-\Delta S_M$ and ΔT_{ad} increase gradually and reach the maximum values (3.28 J/kg·K and 1.62 K for $\Delta H = 45$ kOe). The RCP value of $AlCMn_3$ is 137 J/kg, and 328 J/kg for $\Delta H = 20$, and 45 kOe, respectively (Fig. 6(b)). The RCP value for $\Delta H = 45$ kOe is 1.5 times of that of $GaCMn_3$.

In addition, the MCE of $SnCMn_3$ was studied at the FI–PM transition ($T_C \sim 279$ K). The peak of $-\Delta S_M$ was observed near T_C with the value of 10.28 J/kg·K and 16.84 J/kg·K for $\Delta H = 20$ kOe and 48 kOe, respectively.[45] The $-\Delta S_M$ values are close to that of $GaCMn_3$ (15 J/kg·K) at the first order AFM–IM transition at 159 K. However, the RCP is quite low (28.5 J/kg, $\Delta H = 48$ kOe) due to its first-order nature of the transition. By adjusting the Sn/Mn ratio, the RCP can be remarkably enhanced, accompanying an increase of T_C.[57] For example, the RCP for $Sn_{0.7}CMn_{3.3}$ is 221 J/kg for $\Delta H = 48$ kOe at $T_C \sim 320$ K. Meanwhile, the thermal hysteresis is reduced and the transition at T_C is characterized by a second-order transition.

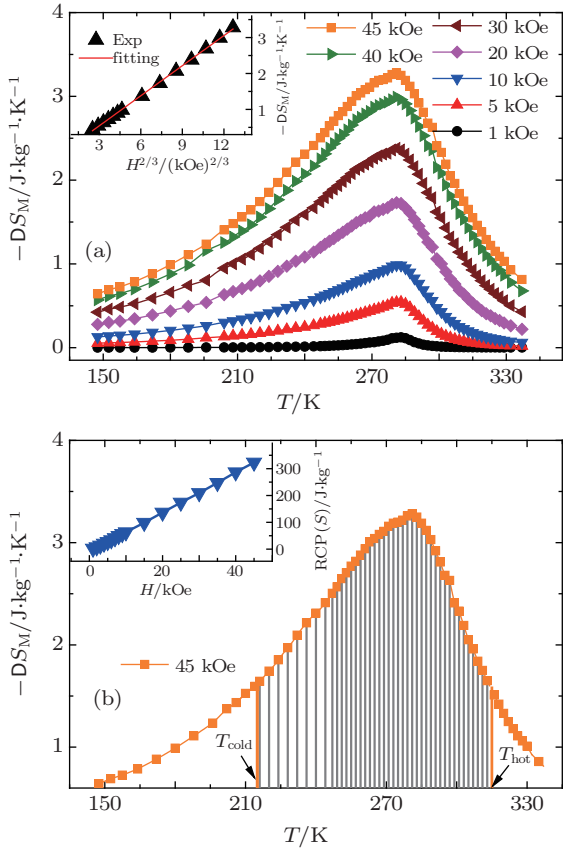


Fig. 6. (a) Magnetic entropy change $-\Delta S_M(T)$ with various magnetic field changes for $AlCMn_3$.[56] Inset shows the maximum magnetic entropy change $-\Delta S_M^{max}$ at T_C as a function of $H^{2/3}$ for $AlCMn_3$. The solid line shows the linear fit to the experimental data. (b) The $-\Delta S_M(T)$ curve for magnetic field change $\Delta H = 45$ kOe. The shaded area is the RCP. The inset shows the magnetic field dependence of RCP.

The RCP values of $Ga_{1-x}CMn_{3+x}$ ($x = 0.6$, 0.7, and 0.8), $Ga_{1-x}Al_xCMn_3$ ($x = 0$, 0.05, 0.07, 0.12, and 0.15), $GaCMn_{3-x}Ni_x$ ($x = 0.05$ and 0.1), $Sn_{1-x}CMn_{3+x}$ ($x = 0.25$ and 0.3), $AlCMn_3$ and several typical magnetic refrigerant materials[58] (such as Gd, $Gd_5Si_2Ge_2$, MnAs, $MnFe_{0.45}As_{0.55}$, and $La_{0.7}Ca_{0.2}Sr_{0.1}MnO_3$) are plotted (see Fig. 7). Regardless of the low magnetic entropy changes, the RCPs of the Mn-based antiperovskite compounds are comparable to those observed in the typical giant MCE materials. The RCP, for instance in $AlCMn_3$, is 80% of that of Gd which is the only material used in most magnetic refrigeration prototypes.[59] Besides the relatively large RCP and adjustable broad working temperature, the antiperovskite $AXMn_3$ compounds have the advantages as a refrigerant material, such as the abundant, low-cost, and non-noxious raw materials, good stability, easy fabrication and shaping, good conductivity, and good mechanical properties. Therefore, the antiperovskite $AXMn_3$ compounds provide a promising alternative material system for pursuing new large-MCE materials at room temperature.

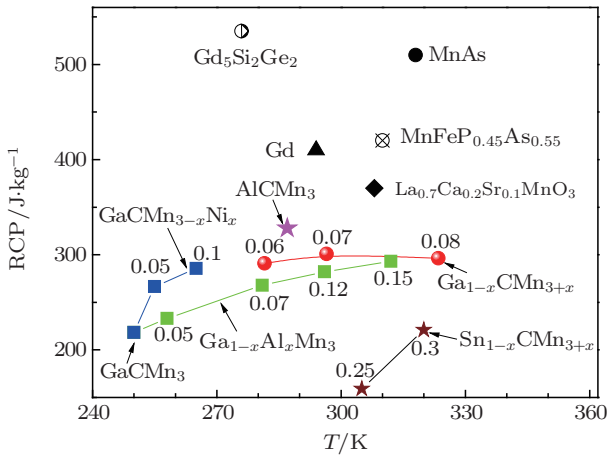


Fig. 7. A comparison of the RCPs of antiperovskite compounds $AlCMn_3$, $Ga_{1-x}Al_xCMn_3$, $Ga_{1-y}CMn_{3+y}$, $GaCMn_{3-x}Ni_x$ (ΔH = 45 kOe), $Sn_{1-y}CMn_{3+y}$ (ΔH = 48 kOe) with those of potential candidates [e.g., Gd, $Gd_5Si_2Ge_2$, MnAs, $MnFe_{0.45}As_{0.55}$, and $La_{0.7}Ca_{0.2}Sr_{0.1}MnO_3$] for magnetic refrigerant (ΔH = 50 kOe).

4. Negative thermal expansion (NTE) with wide temperature span in Mn-based antiperovskite nitrides and a possible mechanism

Usually, most solid materials expand when heated and shrink when cooled. However, though rare, some materials contract on heating, and they are called NTE materials. NTE materials have been the subject of extensive investigation due to their potential in applications where precise control of the thermal expansion is indispensable, as in thermal-expansion compensators.[60] Up to now, most existing NTE materials, with the exception of ZrW_2O_8,[61] are anisotropic. Unfortunately, micro-cracking may be formed due to structural anisotropy during repeated thermal cycling, which hinders the performance of the NTE materials. On the other hand, for many applications, NTE materials with high electrical or thermal conductivity would be desirable,[19] while the isotropic ZrW_2O_8 is ceramic.

Recent progress in the doped antiperovskite nitrides $ANMn_3$ provided a new venue for seeking new metallic isotropic NTE materials.[19–22] The parent $ANMn_3$ compound often shows a large discontinuous volume contraction, hereby referred to as the magneto-volume effect (MVE),[19] accompanied by a sharp first-order transition from a low-temperature AFM state to a high-temperature PM state. Partial doping at the A-site broadens the transition and converts the MVE into an NTE effect with the thermal expansion coefficients varying in a wide range.[60] In 2005, large NET (thermal expansion coefficient $\alpha = -25 \times 10^{-6}$ K^{-1}) was discovered by K. Takenaka *et al.* in $Cu_{1-x}Ge_xNMn_3$.[19] With an increasing Ge doping level, the magnetic phase transition broadens gradually, which gives rise to a large NTE over a wide temperature range. For Ge doping level $x = 0.47$ and 0.50, the NTE coefficients are about -16×10^{-6} K^{-1} (267 K–342 K), -12×10^{-6} K^{-1} (280 K–365 K), respectively. The NTE is isotropic because the cubic symmetry is retained, though the lattice volume changes gradually with temperature. From then on, the NTE effect has been extensively investigated by chemical doping on *A* sites in $ANMn_3$ (*A* = Cu, Zn, Ga, Ni, and etc.).[19–24]

It is interesting that most of the reported NTE or ZTE temperature ranges larger than 100 K do not include room temperature, exempting such substances from general interest for practical applications near room temperature. The reason may lie in the fact that the transition temperature, based on which the NTE or ZTE appears, shifts upward quickly upon chemical doping. For example, in $Cu_{1-x}Sn_xNMn_3$, the AFM transition temperature is increased from around 100 K for $x = 0.1$ to above 400 K for $x = 0.7$.[21] Similar situations can be found in $Cu_{1-x}Ge_xNMn_3$,[19] $Zn_{1-x}Ge_xNMn_3$,[20] and $Zn_{1-x}Sn_xNMn_3$.[62] We reported an effective method to resolve such a problem by pre-decreasing the MVE temperature via chemical alloying, and finally NTE covering low temperatures or room temperature was realized in $Cu_{0.8-y}Sn_yNMn_{3.2}$.[63,64]

As motivated by the experiments for $Ga_{1-x}CMn_{3+x}$[53] and $Sn_{1-x}CMn_{3+x}$[57] where the physical properties depend significantly on Ga/Mn or Sn/Mn ratio, we studied the structural, magnetic, and transport properties in $Cu_{1-x}NMn_{3+x}$ by adjusting the Cu/Mn ratio.[63] For $x = 0.0$, a first-order phase transition from a high temperature PM cubic phase to a low-temperature FI tetragonal phase was observed at T_C (143 K), consistent with the previous report. For $x = 0.1$, T_C is reduced to 119 K and the tetragonality is reduced in the tetragonal phase below T_C. Surprisingly, a new magnetic transition which is second-order without structural transition was observed at 168 K. With increasing x, T_C and the tetragonality are reduced further (Fig. 8(a)), while the second-order transition temperature keeps increasing. The sample with composition $Cu_{0.8}NMn_{3.2}$ was selected to explore NTE behavior by partially replacing Cu with Sn. The temperature-dependent structure for $Cu_{0.8-y}Sn_yNMn_{3.2}$ ($y = 0.1$, 0.2, 0.3, 0.4, and 0.5) was checked by X-ray diffraction.[64] The tetragonality below T_C was completely suppressed by doping level $y = 0.1$ (Fig. 8(b)). Instead of the cubic-tetragonal structural transition, a cubic–cubic transition with sudden lattice expansion was observed for $y = 0.1$ and 0.2. As y increases further, the sudden lattice change broadens and the MVE changes to NTE. The coefficient of linear NTE, α, is about -64.54 ppm/K between 190 K and 235 K for $y = 0.3$. The α value is much larger than the reported values in the antiperovskite NTE materials with similar temperature spans.[19–22] Interestingly, when $y = 0.5$, the NTE effect has a temperature range of 250 K (150 K–400 K) including room temperature. The related coefficient α is -6.8 ppm/K, which is close to that of the typical NTE material α-ZrW_2O_8 (-9 ppm/K, < 425 K).[61] The large temperature span, tunable thermal expansion coefficient,

lattice isotropy, and mechanical hardness make Mn-based antiperovskite NTE compounds promising for commercial applications.

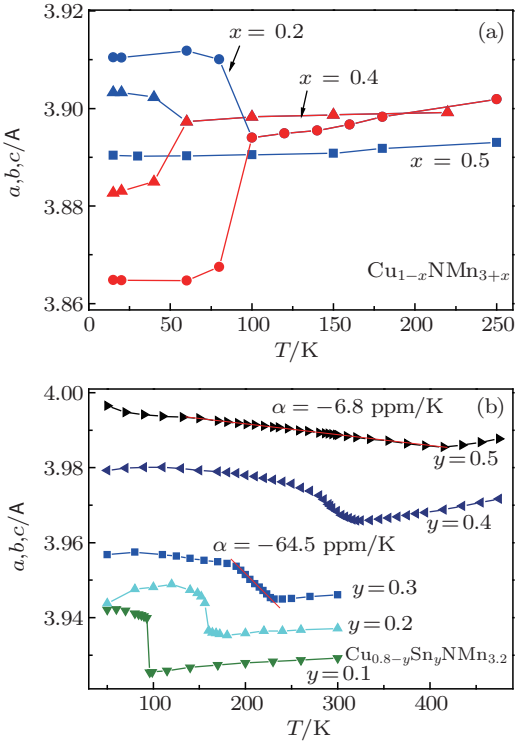


Fig. 8. The evolution of lattice constant with temperature for (a) $Cu_{1-x}NMn_{3+x}$[63] and (b) $Cu_{0.8-y}Sn_yNMn_{3.2}$.[64] The thermal expansion coefficient α is shown for $y = 0.3$ and 0.5.

On the other hand, learning the origin of the NTE in $ANMn_3$ depends on finding out what lies beneath the broadening of the magnetic transition with *A*-site doping. Recent neutron diffraction studies on $Cu_{1-x}Ge_xNMn_3$ indicate that the pronounced MVE occurs only when the non-collinear triangular Γ^{5g} spin structure is realized in the low-temperature AFM state.[65] Further, investigation of the local atomic structure via the neutron Pair Distribution Function (PDF) technique suggest that local lattice distortions give rise to an instability that drives the system towards the symmetry of the end compound $GeNMn_3$ and may in turn be associated with the NTE effect in $Cu_{1-x}Ge_xNMn_3$.[66] Now, the question is whether these distortions are universal in NTE antiperovskites because the local structure information for the other materials is absent.

Recently, we compared the local structure of $Cu_{1-x}Sn_xNMn_3$ with $x = 0.1$ (MVE) and $x = 0.5$ (NTE) through PDF analysis by neutron scattering.[67] The local structure distortion evidenced by the peak splitting at ~ 3 Å was observed at high temperatures as displayed in Fig. 9(a), which cannot be explained by the broadening due to the increased thermal vibrations. Local symmetry lower than the average cubic symmetry was also observed in $Cu_{1-x}Ge_xNMn_3$ and was well described by assuming a local structure based on the $I4/mcm$ symmetry, the average crystal symmetry of the end member $GeNMn_3$.[66] In the $Cu_{1-x}Sn_xNMn_3$, the average symmetry is $P4/mmm$ for both end members, $SnNMn_3$ and $CuNMn_3$. However, a model PDF based on the $P4/mmm$ symmetry fails to reproduce the peak splitting. Therefore, the peak split in $Cu_{1-x}Sn_xNMn_3$ does not originate from a structure instability that gravitates toward the average structure of the end members. Instead, the same $I4/mcm$ symmetry that fits the local distortions in $Cu_{1-x}Ge_xNMn_3$ is able to reproduce the splitting here.

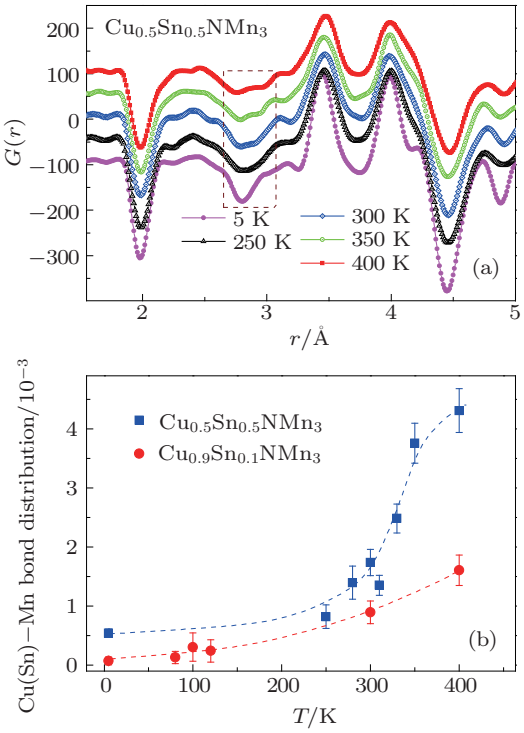


Fig. 9. (a) Pair distribution function $G(r)$ for $Cu_{0.5}Sn_{0.5}NMn_3$ as a function of temperature. The dashed rectangle highlights the Cu/Sn–Mn peak splitting. (b) Cu/Sn–Mn bond distribution as a function of temperature for $Cu_{0.9}Sn_{0.1}NMn_3$ and $Cu_{0.5}Sn_{0.5}NMn_3$.[67]

The $I4/mcm$ symmetry allows three different types of Cu/Sn–Mn bond lengths. By fitting the PDF data to the $I4/mcm$ model, the evolution of each bond length with temperature was obtained for both $x = 0.1$ and 0.5 and the deduced Cu/Sn–Mn bond distribution is shown in Fig. 9(b). It can be seen that the bond distribution is enhanced at high temperatures, more markedly in x= 0.5 than in $x = 0.1$. The Γ^{5g} AFM state is thought to be crucial for the occurrence of the NTE in the $ANMn_3$. Otherwise, the hybridization between the p state of the dopants (such as Sn and Ge) and the Mn 3d states was proposed to be important for stabilizing the Γ^{5g} AFM ground state.[31] Since the Cu/Sn–Mn bond length is directly related to the strength of the Cu/Sn p–Mn d orbital hybridization, the distributed Cu/Sn–Mn bonds indicates the fluctuation in strength of the Γ^{5g} AFM exchange integrals. The fluctuating AFM exchange integrals would distribute the ordering temperature when the system is cooled down. At higher Sn doping level, the wider spread of Cu/Sn–Mn bonds will give

rise to a larger distribution of ordering temperatures that may explain the broader magnetic transition in $x = 0.5$. Similarly, a recent X-ray absorption fine structure (XAFS) measurement shows that the Cu–Mn bond is much longer than the Ge–Mn bond in the NTE material of $Cu_{0.7}Ge_{0.3}NMn_3$, while the Ag–Mn and Cu–Mn bonds in the MVE system of $Cu_{0.7}Ag_{0.3}NMn_3$ are close to each other.[68] We note that the magnetic transition broadening (or say the NTE) synchronizes with the elongation of magnetic moment upon cooling,[67] which may correspond to a wide dip below T_N in the inverse bulk magnetic susceptibility $1/\chi(T)$.[69] The above discussion also gives insight into the mechanism for magneto-structural coupling at the magnetic transition.

Experimentally, it is found that the NTE associated with the magnetic transition broadening has been widely observed so far in the solid solutions with two p electrons,[67] such as in Sn- or Ge-doped $CuNMn_3$, Sn- or Ge-doped $ZnNMn_3$, and $Ga_{1-x}Si_xNMn_3$. However, the solid solutions without or with only one p electron (e.g., Zn-, or Ag-, or Ga-doped $CuNMn_3$) do not exhibit such kind of NTE. This reality may strengthen the scenario proposed above that the magnetic transition broadening is closely related with the fluctuating A p–Mn d hybridization in *A*-site doped $ANMn_3$. The current result proposes a possible mechanism for the NTE with magnetic/structural transition broadening in doped $ANMn_3$ compounds, which links the experimental results and theoretical predictions and provides some hints for exploring better NTE materials based on the magneto-structural coupling.[67]

5. Adjustable nearly zero temperature coefficient of resistivity (TCR) in $CuN_{1-x}C_xMn_3$ and $CuNMn_{3-y}Co_y$

The materials with low TCR play an important role in electronic equipment such as normal resistors in high-precision electronic apparatus, anti-surge resistors in high power applications, and various functional sensors. Now days, the low-TCR Ni–Cr alloys,[70] Manganin,[71] Ru-containing compounds[72] are used commercially. However, these materials still have some shortcomings. For instance, the Cr ions pollute the environment and Cr^{6+} is virulent. Ruthenium increases the cost of Ru-containing compounds. Thus it is interesting to seek new types of low-TCR materials that can overcome the above problems in the low TCR materials currently in use.

The low TCR discovered in antiperovskite $CuNMn_3$ in 2001 opened a new scope for this purpose.[25] Above the magnetic/structural transition $T_C \sim 143$ K, the resistivity is barely temperature-dependent, and the TCR value, defined by $\rho_0^{-1}(d\rho/dT)$, where ρ_0 is the resistivity at 273 K, is 46 ppm/K. This value is about two orders of magnitude smaller than those of pure metals like Cu and Al, and close to that of typical zero-TCR materials with TCR less than 25 ppm/K. Subsequently, chemical doping has been applied to improve the TCR effect in antiperovskite $ANMn_3$ (A = Cu, Ni, Ag, Co, Zn, and etc.) with great success. For example, in $Ag_{1-x}Cu_xNMn_3$, the optimized TCR value is only about 1 ppm/K, (294 K–304 K) or 6 ppm/K (280 K–322 K).[26] For $Cu_{0.3}Ni_{0.7}NMn_3$, the TCR is 22 ppm/K (260 K–360 K), while for $Cu_{0.5}Ni_{0.5}NMn_3$ this value is reduced to 0.09 ppm/K with a narrowed temperature region (300 K–330 K).[27] All the reported experimental results are focused on *A* site doping. Considering that the electronic DOS at E_F is mainly from Mn 3d state and the strong N-2p Mn-3d hybridization, the doping on N or on Mn sites is expected to modify the physical properties of $ANMn_3$. Therefore, we investigated the effects of C substitution for N and Co substitution for Mn on the TCR in $CuNMn_3$.[73]

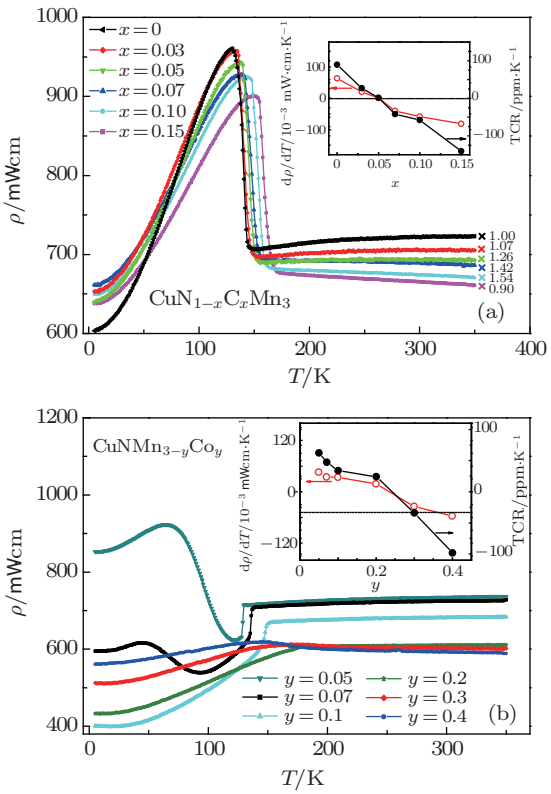


Fig. 10. (a) Temperature-dependent resistivity for $CuN_{1x}C_xMn_3$ between 5 K and 350 K. For the sake of clarity, some constant values (shown at the end of each curve) are added to the resistivity data. Inset: the x dependence of TCR and $d\rho/dT$ for $CuN_{1x}C_xMn_3$. (b) Temperature-dependent resistivity for $CuNMn_{3y}Co_y$ between 5 K and 350 K. Inset: the y dependence of TCR and $d\rho/dT$ for $CuNMn_{3y}Co_y$.[73]

Temperature dependence of resistivity is shown in Fig. 10 for both series. For $CuN_{1-x}C_xMn_3$, T_C increases monotonically with x and the $\rho(T)$ shape is kept. A similar trend of T_C was found in $CuNMn_{3-y}Co_y$, but the $\rho(T)$ below T_C depends strongly on y. Although the $\rho(T)$ curves are not a perfect straight-line in the whole temperature range between T_C and 350 K, a quasi-straight-line was observed around room

temperature for each sample. The derived TCR is summarized in the inset of Fig. 10. For both series, the TCR is found to decrease monotonically from positive to negative as the doping level increases. Extremely low TCR was observed when the composition approaches the critical points. For example, the TCR value is only 1.29 ppm/K between 240 K and 320 K in $x = 0.05$ sample (i.e., $CuN_{0.95}C_{0.05}Mn_3$), which is less than the typical value for nearly zero TCR materials ($\sim$ 25 ppm/K) and that for manganin by one order of magnitude. In fact, the TCR can be further reduced by precisely controlling the carbon content within $0.05 \leq x \leq 0.07$ or the cobalt content within $0.2 \leq y \leq 0.3$. Furthermore, the thermal stability of current materials is guaranteed for potential applications of the TCR since neither thermal hysteresis nor resistivity jump is observed during the cyclic temperature changes above T_C.[74] Taking into account the advantages of the antiperovskite $ANMn_3$ materials mentioned in above sections, the current systems possess a giant prospect of commercial applications.

In spite of the great progress in experiments, we still know rather little about the origin of the low TCR observed in antiperovskite $ANMn_3$ compounds. In $CuNMn_3$, the low TCR was phenomenologically attributed to the low resistivity slop $d\rho(T)/dT$ in combination with the large ρ_0.[25] However, the authors in Ref. [25] also pointed that the origin of TCR differs essentially from that observed in disordered metal. In $NiNMn_3$, both the carrier mobility and the carrier density were thought to be temperature-dependent, a delicate balance between them above the magnetic/structural transition accounts for the low TCR. In $Ag_{1-x}Cu_xNMn_3$, a broad maximum appears in the $\rho(T)$ curve in the PM region, and the extremely low TCR is closely related with such an abnormality in $\rho(T)$. The peak position is obviously associated with the magnetic transition. A possible collapse of coherent quasiparticle states by strong magnetic scattering was speculated to be responsible for the broad maximum in $\rho(T)$ and the nearly zero TCR.[26] Further, it was proposed that the short range spin order in the PM state exhibits a negative temperature dependence that compensates for the positive contribution from phonon scattering, and consequently gives rise to a nearly temperature-independent resistivity.[27] As displayed in the insets of Fig. 10, the TCR and $d\rho/dT$ share similar dependencies on Co or C concentration. This implies that the low TCR in our case is closely related to the temperature dependence of resistivity. For $CuNMn_{3-x}Co_x$ series, a clear deviation of $1/\chi(T)$ curve from linear temperature dependence (the Curie–Weiss law) can be found in a large temperature region just above T_C.[74] It is probably indicative of short-range magnetic clusters existing above T_C. It may back up the scenario that the scattering of conduction charges due to magnetic clusters would counteract the increasing phonon scattering as temperature increases. Despite the above models proposed by different authors, a uniform understanding of the low TCR is still absent, and thus further work, especially theoretical calculation, is desirable for elucidating the nature of low TCR observed in antiperovskite nitrides $ANMn_3$.

6. Electronic itinerancy and hybridization between X-p and Mn-3d states in Mn-based antiperovskite $AXMn_3$

Due to the X p–Mn d hybridization which forms a wide conduction band, it has been widely accepted that magnetism in $AXMn_3$ is itinerant in nature.[30] Indeed, it is often observed that the magnetic moment in $AXMn_3$ is much weaker than that observed in manganites where the magnetism originates from localized moments. In fact, there are some compounds that show large magnetic moments, and in some compounds the moment varies between the different magnetic states.[4] Furthermore, models (e.g., Heisenberg model) based on localized moments were proposed to explain the experimental results and sometimes worked.[15] Surprisingly little attention has been given so far to such a divergence with respect to the magnetic mechanisms in these compounds. Our recent work tried to discuss this issue from different aspects.

Critical exponents study by analyzing the field-dependent magnetization in the vicinity of magnetic transition can give an insight into the microscopic interactions responsible for magnetic transitions.[75] The second-order FM phase transition near the Curie point is characterized by a set of critical exponents, β (associated with the spontaneous magnetization), γ (relevant to the initial magnetic susceptibility), and δ (associated with the critical magnetization isotherm).[76] We studied the critical scaling behavior around the FM transition for some Mn-based antiperovskite carbides, such as $AlCMn_3$[77] and $GaCMn_3$.[78] For $AlCMn_3$, reliable critical components β and γ were estimated by using the modified Arrott plot and the Kouvel–Fisher method, and the component δ was determined by critical isothermal analysis. The obtained values of β, γ, and δ are very close to those expedited by the mean-field model, indicative of a long-range FM interaction in $AlCMn_3$. Consistently, the saturated magnetization ($\sim$ 1.2 μ_B/Mn) is quite small when it is compared with manganites (3 μ_B/Mn–4 μ_B/Mn). The linear dependence of the maximum magnetic entropy change $-\Delta S_M^{max}$ on $H^{2/3}$ for $AlCMn_3$ also features a second-order FM transition under the framework of mean-field theory.[56] The itinerant FM interactions between Mn atoms are most likely mediated through the intermediate C atom, which corresponds to the wide conduction band due to the C 2p–Mn 3d hybridization. However, the obtained β and γ values are slightly larger than those predicted. Moreover, for $AlCMn_3$, the long-range magnetic interaction decays as $J(r) \sim r^{-4.7}$, which is between the decay patterns predicted by

the mean-field model and the Heisenberg model. Therefore, the above results strongly suggest the competition between the localized Mn–Mn interactions and the long-range interactions through Mn–C–Mn channels which corresponds to the itinerant electronic band. Similar result was obtained for $GaCMn_3$ based on the analysis of the critical scaling behavior around the FM transition at 250 K.[78]

A direct way to study the X p–Mn d hybridization is to introduce deficiency of X in the $AXMn_3$ lattice. We investigated this issue in nitride $AlNMn_3$[79,80] and carbide $AlCMn_3$.[81] Samples with nominal compositions AN_xMn_3 ($x = 1$, 1.1, and 1.2) were synthesized and their physical properties were checked.[79] All samples show metallic FM behavior and T_C decreasing with increasing x: 818 K, 802 K, and 774 K for $x =$ 1, 1.1, and 1.2, respectively (Fig. 11, upper inset). No structural transition was observed at T_C. Interestingly, the transition temperatures of AlN_xMn_3 are much higher than that of Mn_4N (about 745 K),[6] which may be the highest one among the Mn-based antiperovskite compounds. The resistivity shows a quadratic temperature dependence below 30 K with the expression $\rho(T) - \rho_0 = AT^2$. The Kadowaki–Woods (KW) ratio A/γ^2 that links the resistivity and electronic specific heat (γ) gives a measure of electron–electron correlations.[82] The KW ratio is $10.8a_0$, $1.9a_0$, and $0.4a_0$ for $x = 1$, 1.1, and 1.2 respectively. Here a_0 equals 10 $\mu\Omega$·cm/K^2 which is the universal value for the heavy Fermion systems. The large a_0 values indicate a strong electron–electron correlation in current systems.

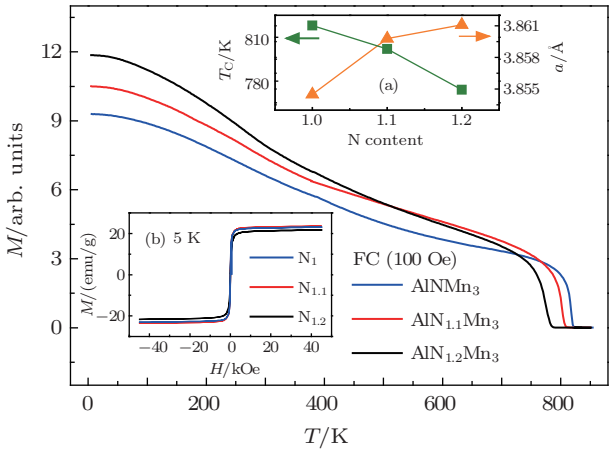


Fig. 11. $M(T)$ under field cooling process at 100 Oe from 5 K to 850 K for AlN_xMn_3 ($x = 1$, 1.1, and 1.2). Top inset: the refined lattice parameter a and the Curie temperature T_C for AlN_xMn_3. Bottom inset: isotherm magnetization curves $M(H)$ at 5 K for AlN_xMn_3.[79]

For further study of the experimental results, we performed a theoretical calculation of the magnetic properties for AlN_xMn_3 by using pseudopotential plan-wave method. Details of the calculation can be found in Ref. [80]. It is found that in the nonmagnetic state, the band from -4 eV to 2 eV are mainly from the Mn-3d electrons with considerable hybridization between N-2p and Mn-3d states, in agreement with the metallic character observed experimentally. The Fermi level resides just at a DOS peak, leading to a high $N(E_F)$ of 8 states/eV. Such a high $N(E_F)$ can lead to magnetic instability. With increasing the N deficiency, the spin-down states move remarkably toward the higher energy (Fig. 12), which enhances the exchange splitting. Furthermore, the N deficiency reduces the N–Mn hybridization, which makes the 3d electrons of Mn tend to occupy the spin-up state and the narrowing of the Mn-d bands. Consequently, the spin polarization is enhanced in N deficient samples, which increases T_C. The reduced electronic itinerancy explains the enhanced resistivity in the whole temperature range with reducing N concentration.[79] By using the Mohn-Wohlfarth model, the T_C was estimated for AlN_xMn_3. By comparing the calculated T_C with the experimental ones, the estimated real x composition in nominal compositions AN_xMn_3 with $x = 1$, 1.1, and 1.2 is between 0.92 and 0.95. In addition, our result indicates the magnetism in $AlNMn_3$ can be described by spin fluctuations. It may explain the strong electron–electron correlations suggested by the large KW ratios.[79] The large spin fluctuations in the FM are also presented by the large low-temperature electronic specific heat constant.[37]

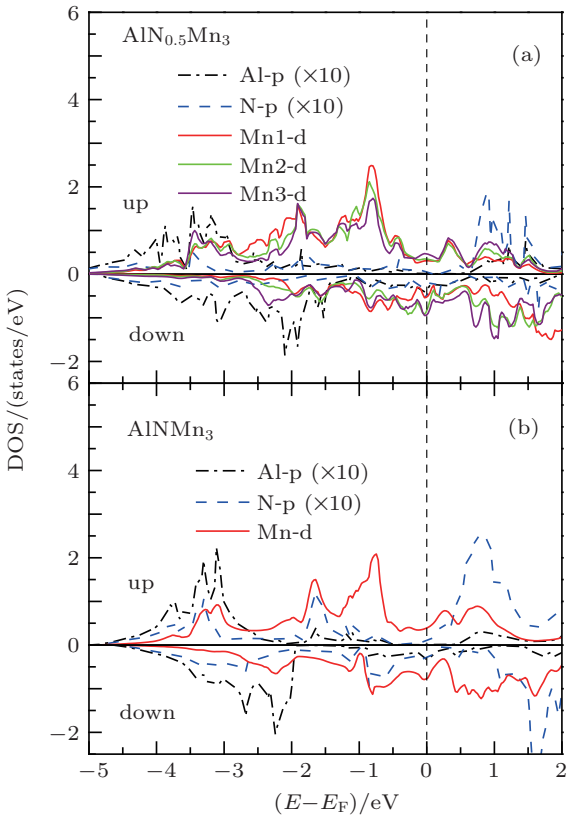


Fig. 12. The projected DOS for AlN_xMn_3 with FM states for (a) $x = 0.5$ and (b) $x = 1$.[80]

In our early experiment on AlC_xMn_3, the FM transition temperature T_C was found to increase initially and then decrease with further increasing x.[81] The competition between

the bandwidth broadening due to C 2p–Mn 3d hybridization and the bandwidth narrowing due to the lattice expansion was suggested to account for the evolution of T_C with carbon concentration.

In addition to the dominant itinerant electron mechanism, our initial experimental results show the magnetic behaviors closely related to the localized-electron scenario. The contribution from the latter mechanism to the magnetism in $AXMn_3$ may be varied from one compound to another. However, this issue is essentially coupled with the origins for the functionalities as introduced in the above sections. Therefore, it is necessary to make a more systematic investigation of the magnetic interactions, employing more techniques (e.g., inelastic neutron scattering).

7. Summary and outlook

Our recent research progress on the Mn-based antiperovskite compounds is summarized as follows.

(i) We systematically explored the MCE in Mn-based antiperovskite carbides. The large RCPs are comparable to those of typical magnetic refrigerant materials (e.g., Gd).

(ii) Compared with parent $GaCMn_3$, enhanced GMR up to 70% at 50 kOe with larger temperature span was observed in $Ga_{1-x}Zn_xCMn_3$ and $GaCMn_{3-x}Ni_x$. The enhanced GMR can be attributed to the weakened AFM background, which favors a field induced AFM–FI/FM transition, though the detailed mechanisms of field-driving magnetic transition are different in the two cases.

(iii) By pre-reducing the cubic-tetragonal transition temperature by means of increasing the Mn concentration in $Cu_{1-x}NMn_{3+x}$, NTE was finally achieved in $Cu_{0.8-y}Sn_yNMn_{3.2}$ at low temperature ($\alpha = -64.54$ ppm/K, between 190 K and 235 K for $y = 0.3$) or around room temperature ($\alpha = -6.8$ ppm/K, between 150 K and 400 K for $y = 0.5$). Our neutron PDF result suggests the NTE in $Cu_{0.5}Sn_{0.5}NMn_3$ is associated with the fluctuation in Cu/Sn–Mn bond length which broadens the AFM transition.

(iv) In $CuN_{1-x}C_xMn_3$ and $CuNMn_{3-y}Co_y$, TCR was found to decrease monotonically from positive to negative as the Co or C content increases. Extremely low TCR is observed when the composition approaches the critical points. For example, TCR value is ~ 1.29 ppm/K between 240 K and 320 K in $CuN_{0.95}C_{0.05}Mn_3$, which one twentieth of that in the typical zero-TCR materials (~ 25 ppm/K).

(v) We demonstrated by studying the critical scaling exponents that, at least for the carbides, the magnetism can be mainly explained by the itinerant scenario. However, the contribution from the localized electrons is not trivial. As an example, nitrogen deficiency was found to reduce the N 2p–Mn 3d hybridization, and thus to reduce the electronic itinerancy. As a result, both the resistivity and T_C were increased. Besides, T_C values observed in deficient AlN_xMn_3 are higher than 800 K, which could be the highest one reported so far in this type of compounds.

Despite an appreciable amount of experimental and computation work devoted to the Mn-based antiperovskite compounds, the mechanism and driving force underlying the functionalities still remain unclear. Microscopic probes, such as neutron diffraction and scattering, are needed to shed light on the correlation among lattice, spin, and charge carriers and the various magnetic couplings, as well as on the possible geometric frustration as proposed in Ref. [34]. Local structural distortion, which has been proved to be crucial for understanding the NTE, may play similarly important roles in determining the other physical properties – a proposition which needs to be clarified in the future. Although actual growth of single crystals is still a challenge at present, success in this would bring a better understanding of the physics in $AXMn_3$. In addition, thin films are the fundamental building blocks of heterojunctions and many nanodevices, and offer more options for controlling physical properties than do the bulk samples. Therefore, the Mn-based antiperovskite thin films and related physics are sure to become an attractive research field in the near future.

Acknowledgements

Drs. Lu Wen-Jian, Zhang Lei, Lin Jian-Chao, Lin Shuai and Shao Ding-Fu are acknowledged for their valuable discussions.

References

[1] Bednorz J G and Mueller K A 1986 *Z. Phys. B: Condens. Matter* **64** 189
[2] Ahn C H, Tybell T, Antognazza L, Char K, Hammond R H, Beasley M R, Fischer O and Triscone J M 1997 *Science* **276** 1100
[3] Nagaev E L 2001 *Phys. Rep.* **346** 387
[4] Fruchart D and Bertaut E F 1978 *J. Phys. Soc. Jpn.* **44** 781
[5] Fruchart D, Bertaut E F, Sayetat F, Eddine M N, Fruchart R and Sénateur J P 1970 *Solid State Commun.* **8** 91
[6] Takei W J, Heikes R R and Shirane G 1962 *Phys. Rev.* **125** 1893
[7] Kenmotsu A, Shinohara T and Watanabe H 1972 *J. Phys. Soc. Jpn.* **32** 377
[8] Khoi L D, Fruchart M E and Fruchart M R 1970 *Solid State Commun.* **8** 49
[9] Navarro R, Rojo J A, García J, González D, Bartolomé J and L'Héritier Ph 1986 *J. Magn. Magn. Mater.* **59** 221
[10] Bouchaud J P, Fruchart R, Pauthenet R, Guillot M, Bartholin H and Chaissé F 1966 *J. Appl. Phys.* **37** 971
[11] L'Héritier Ph, Boursier D, Fruchart R and Fruchart D 1979 *Mater. Res. Bull.* **14** 1203
[12] Keneko T, Kanomata T, Miura S, Kido G and Nakagawa Y 1987 *J. Magn. Magn. Mater.* **70** 261
[13] He T, Huang Q, Ramirez A P, Wang Y, Regan K A, Rogado N, Hayward M A, Haas M K, Slusky K S, Inumara K, Zandbergen H W, Ong P N and Cava R J 2001 *Nature* (London) **411** 54
[14] Kamishima K, Goto T, Nakagawa H, Miura N, Ohashi M, Mori N, Sasaki T and Kanomata T 2000 *Phys. Rev. B* **63** 024426

[15] Li Y B, Li W F, Feng W J, Zhang Y Q and Zhang Z D 2005 *Phys. Rev. B* **72** 024411
[16] Yu M H, Lewis L H and Moodenbaugh A R 2003 *J. Appl. Phys.* **93** 10128
[17] Tohei T, Wada H and Kanomata T 2004 *J. Magn. Magn. Mater.* **272–276** e585
[18] Sun N K, Li Y B, Liu F and Ji T B 2012 *J. Mater. Sci. Technol.* **28** 941
[19] Takenaka K and Takagi H 2005 *Appl. Phys. Lett.* **87** 261902
[20] Sun Y, Wang C, Wen Y C, Zhu K G and Zhao J T 2007 *Appl. Phys. Lett.* **91** 231913
[21] Takenaka K, Asano K, Misawa M and Takagi H 2008 *Appl. Phys. Lett.* **92** 011927
[22] Huang R J, Li L F, Cai F S, Xu X D and Qian L H 2008 *Appl. Phys. Lett.* **93** 081902
[23] Wang C, Chu L H, Yao Q R, Sun Y, Wu M M, Ding L, Yan J, Na Y Y, Tang W H, Li G N, Huang Q Z and Lynn J W 2012 *Phys. Rev. B* **85** 220103
[24] Song X Y, Sun Z H, Huang Q Z, Rettenmayr M, Liu X M, Seyring M, Li G N, Rao G H and Yin F X 2011 *Adv. Mater.* **23** 4690
[25] Chi E O, Kim W S and Hur N H 2001 *Solid State Commun.* **120** 307
[26] Takenaka K, Ozawa A, Shibayama T, Kaneko N, Oe T and Urano C 2011 *Appl. Phys. Lett.* **98** 022103
[27] Ding L, Wang C, Chu L H, Yan J, Na Y Y, Huang Q Z and Chen X L 2011 *Appl. Phys. Lett.* **99** 251905
[28] Asano K, Koyama K and Takenaka K 2008 *Appl. Phys. Lett.* **92** 161909
[29] Nakamura Y, Takenaka K, Kishimoto A and Takagi H 2009 *J. Am Ceram. Soc.* **92** 2999
[30] Shim J H, Kwon S K and Min B I 2002 *Phys. Rev. B* **66** 020406
[31] Hua L, Wang L and Chen L F 2010 *J. Phys.: Condens. Matter* **22** 206003
[32] Lewis L H, Yoder D, Moodenbaugh A R and Yu M H 2006 *J. Phys.: Condens. Matter* **18** 1677
[33] Kim W S, Chi E O, Kim J C, Choi H S and Hur N H 2001 *Solid State Commun.* **119** 507
[34] Tahara D, Motome Y and Imada M 2007 *J. Phys. Soc. Jpn.* **76** 013708
[35] Takenaka K, Inagaki T and Takagi H 2009 *Appl. Phys. Lett.* **95** 132508
[36] Kaneko T, Kanomata T and Shirakawa K 1987 *J. Phys. Soc. Jpn.* **56** 4047
[37] Kamishima K, Bartashevich M I, Goto T, Kikuchi M and Kanomata T 1998 *J. Phys. Soc. Jpn.* **67** 1748
[38] Wang B S, Tong P, Sun Y P, Li L J, Tang W, Lu W J, Zhu X B, Yang Z R and Song W H 2009 *Appl. Phys. Lett.* **95** 222509
[39] Wang B S, Li C C, Lin J C, Lin S, Tong P, Zhu X B, Zhao B C, Lu W J, Yang Z R, Song W H, Dai J M and Sun Y P 2010 *Appl. Phys. Lett.* **97** 142505
[40] Chattopadhyay M K and Roy S B 2008 *J. Phys.: Condens. Matter* **20** 025209
[41] Zhang Y Q, Zhang Z D and Aarts J 2004 *Phys. Rev. B* **70** 132407
[42] Yu S Y, Liu Z H, Liu G D, Chen J L, Cao Z X, Wu G H, Zhang B and Zhang X X 2006 *Appl. Phys. Lett.* **89** 162503
[43] Zhang Y Q and Zhang Z D 2003 *Phys. Rev. B* **67** 132405
[44] Wang B S, Tong P, Sun Y P, Song W H, Yang Z R and Dai J M 2009 *J. Appl. Phys.* **106** 013906
[45] Wang B S, Tong P, Sun Y P, Luo X, Zhu X B, Li G, Zhu X D, Zhang S B, Yang Z R, Song W H and Dai J M 2009 *Europhys. Lett.* **85** 47004
[46] Wang B S, Tong P, Sun Y P, Tang W, Li L J, Zhu X B, Yang Z R and Song W H 2010 *J. Magn. Magn. Mater.* **322** 163
[47] Shen B G, Sun J R, Hu F X, Zhang H W and Cheng Z H 2009 *Adv. Mater.* **21** 4545
[48] Pecharsky V K and Gschneidner K A Jr 1997 *Phys. Rev. Lett.* **78** 4494
[49] Wada H and Tanabe Y 2001 *Appl. Phys. Lett.* **79** 3302
[50] Hu F X, Shen B G, Sun J R and Zhang X X 2000 *Chin. Phys.* **9** 550
[51] Guo Z B, Du Y W, Zhu J S, Huang H, Ding W P and Feng D 1997 *Phys. Rev. Lett.* **78** 1142
[52] Liu J, Gottschall T, Skokov K P, Moore J D and Gutfleisch O 2012 *Nat. Mater.* **11** 620
[53] Wang B S, Tong P, Sun Y P, Zhu X B, Luo X, Li G, Song W H, Yang Z R and Dai J M 2009 *J. Appl. Phys.* **105** 083907
[54] Wang B S, Li C C, Lin S, Lin J C, Tong P, Lu W J, Zhu Z B, Yang Z R, Song W H, Dai J M and Sun Y P 2011 *J. Magn. Magn. Mater.* **323** 2017
[55] Wang B S, Tong P, Sun Y P, Tang W, Li L J, Zhu X B, Yang Z R and Song W H 2010 *Physica B* **405** 2427
[56] Wang B S, Lin J C, Tong P, Zhang L, Lu W J, Zhu X B, Yang Z R, Song W H, Dai J M and Sun Y P 2010 *J. Appl. Phys.* **108** 093925
[57] Wang B S, Lu W J, Lin S, Lin J C, Tong P, Song W H and Sun Y P 2012 *J. Magn. Magn. Mater.* **324** 773
[58] Tishin A M 2007 *J. Magn. Magn. Mater.* **316** 351
[59] Yu B F, Liu M, Egolf P W and Kitanovski A 2010 *Int. J. Refrigeration* **33** 1029
[60] Takenaka K 2012 *Sci. Technol. Adv. Mater.* **13** 013001
[61] Mary T A, Evans J S O, Vogt T and Sleight A W 1996 *Science* **272** 90
[62] Sun Y, Wang C, Wen Y C, Chu L H, Pan H and Nie M 2010 *J. Am. Ceram. Soc.* **93** 2178
[63] Lin J C, Wang B S, Lin S, Tong P, Lu W J, Zhang L, Zhao B C, Song W H and Sun Y P 2012 *J. Appl. Phys.* **111** 113914
[64] Lin J C, Wang B S, Lin S, Tong P, Lu W J, Zhang L, Song W H and Sun Y P 2012 *J. Appl. Phys.* **111** 043905
[65] Iikubo S, Kodama K, Takenaka K, Takagi H and Shamoto S 2008 *Phys. Rev. B* **77** 020409
[66] Iikubo S, Kodama K, Takenaka K, Takagi H, Takigawa M and Shamoto S 2008 *Phys. Rev. Lett.* **101** 205901
[67] Tong P, Louca D, King G, Llobet A, Lin J C and Sun Y P 2013 *Appl. Phys. Lett.* **102** 041908
[68] Matsuno J, Takenaka K, Takagi H, Matsumura D, Nishihata Y and Mizuki J 2009 *Appl. Phys. Lett.* **94** 181904
[69] Takenaka K and Takagi H 2006 *Mater. Trans.* **47** 471
[70] Phuong N M, Kim D J, Kang B D, Kim C S and Yoon S G 2006 *J. Electrochem. Soc.* **153** G27
[71] Kuo C C Y 1996 16*th Capacitor and Resistor Technology Symposium* **1996** CARTS '96, p. 266
[72] Kagomiya I, Matsumoto S, Kakimoto K, Ohsato H, Sakai H and Maeda Y 2009 *Mater. Lett.* **63** 2452
[73] Lin J C, Wang B S, Tong P, Lin S, Lu W J, Zhu X B, Yang Z R, Song W H, Dai J M and Sun Y P 2011 *Scr. Mater.* **65** 452
[74] Lin J C, Tong P, Wang B S, Lin S, Lu W J, Zhao B C and Sun Y P 2013 *Phys. Express* **3** 33
[75] Heller P 1967 *Rep. Prog. Phys.* **30** 731
[76] Yang J, Lee Y P and Li Y 2007 *Phys. Rev. B* **76** 054442
[77] Zhang L, Wang B S, Sun Y P, Tong P, Fan J Y, Zhang C J, Pi L and Zhang Y H 2012 *Phys. Rev. B* **85** 104419
[78] Wang B S 2011 Study on the Physical Properties of Manganese Based Antiperovskite Carbon Compounds (Ga, Al, Sn)CMn_3 (Ph. D. Dissertation) (Hefei: Chinese Academy of Sciences) (in Chinese)
[79] Lin J C, Wang B S, Tong P, Sun Y P, Zhu X B, Yang Z R, Song W H and Dai J M 2011 *Appl. Phys. Lett.* **98** 092507
[80] Shao D F, Lu W J, Lin J C, Tong P, Jian H B and Sun Y P 2013 *J. Appl. Phys.* **113** 023905
[81] Tong P, Sun Y P, Zhao B C, Zhu X B and Song W H 2006 *Solid State Commun.* **138** 64
[82] Tong P, Sun Y P, Zhu X B and Song W H 2006 *Phys. Rev. B* **73** 245106